Materials Today Physics 49 (2024) 101582

Contents lists available at ScienceDirect

Materials Today Physics

journal homepage: www.journals.elsevier.com/materials-today-physics

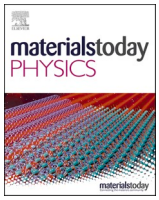

Infinitely rugged intra-cage potential energy landscape in metallic glasses caused by many-body interaction

Haoyu Li [a], Hongyi Xiao [a], Takeshi Egami [b,c], Yue Fan [a,*]

[a] Department of Mechanical Engineering, University of Michigan, Ann Arbor, USA
[b] Department of Materials Science and Engineering and Department of Physics and Astronomy, University of Tennessee, Knoxville, USA
[c] Materials Science and Technology Division, Oak Ridge National Laboratory, Oak Ridge, USA

ARTICLE INFO

Keywords:
Potential energy landscape
Infinite ruggedness
Interior of sub-basins
Many-body interacting glasses
Irreversibility
Intra-cage cyclic loading

ABSTRACT

The absence of translational symmetry in glassy materials poses a significant challenge in establishing effective structure-property relationships in real space. Consequently, the potential energy landscape (PEL) in phase space is widely utilized to comprehend the complex phenomena in glasses. The classical PEL features a two-scale profile comprising mega-basins and sub-basins, corresponding to α-relaxations (*e.g.* glass transition) and β-relaxations (*e.g.* local cage-breaking atomic rearrangements), respectively. Recent studies, however, reveal that sub-basins are not smooth and contain finer structures, the origins of which remain elusive. Here we probe the smoothness of sub-basin bottoms in glasses' PEL by introducing small intra-cage cyclic loading and then measuring the net changes in atomic-level stresses. Compared to glasses with pair interaction, glasses with many-body interaction exhibit orders-of-magnitude larger and loading-dependent stress changes even before the first cage-breaking event takes place, which reflect much more feature-rich sub-basins. We further demonstrate this stark contrast stems from the spatial distribution of individual atom's constraining force field. Specifically, at vanishing perturbations, many-body interactions disrupt the positive-definite synchrony in energy variations of the perturbed atom and the whole system, causing inherently less confined atomic responses and infinitely rugged sub-basins. The implications of these findings for the selective addition or removal of fine structures in the PEL and the subsequent tuning of glassy materials' responses to external stimuli are also explored.

1. Introduction

Understanding physical and mechanical behaviors of amorphous materials holds considerable significance, both from scientific and practical perspectives, for a diverse array of systems encompassing broad scales from metallic glasses [1–4], to polymers [5–7], colloids [8,9], foams [10], and granular materials [11]. Due to their inherently disordered atomic packing, it is immensely challenging to build unambiguous structure-property relationship. Among various efforts and models developed, the approach of potential energy landscape (PEL) offers a unique and, in principle, fundamental perspective to probe the system's behavior in hyper-dimensional phase space – for the reason that it can alleviate the empirical assumptions of "structural defects" in disordered matters (*e.g.* flow units, geometrically unfavorable motifs, free volumes, *etc*). The current consensus on PEL in glassy materials is that it exhibits a two-scale mega-basin/sub-basin landscape [12–14]. Upon sufficient external energy input (*e.g.* by high temperature and/or applied stress), transitions between mega-basins – also known as α relaxations – can be activated, which would cause system-level property changes such as glass transition; while under relatively weak thermo-mechanical stimuli, only β relaxations – namely the transitions between neighboring sub-basins via local cage-breaking atomic rearrangements [15–17] – are permissible, causing spatially isolated elementary plasticity events and the signatures such as excess wings or peaks in the spectra of dynamic mechanical analysis (DMA) measurements [17–19]. Note that the activation barriers for β relaxations are broadly distributed and could be very low in many cases [3,20].

Within such a classical PEL picture, if external stimuli are vanishingly small – namely much lower than the separating barriers between neighboring sub-basins – then β relaxations would also be prohibited, effectively freezing the system in a sub-basin and suppressing any dissipating processes. However, experiments manifest the so-called nearly constant loss (NCL) phenomenon even at low temperature limit [15,21] or in the early linear elastic regime far below the mechanical

* Corresponding author.
E-mail address: fanyue@umich.edu (Y. Fan).

https://doi.org/10.1016/j.mtphys.2024.101582
Received 25 September 2024; Received in revised form 30 October 2024; Accepted 1 November 2024
Available online 6 November 2024

instability regime [22,23], suggesting an intricate picture inside an individual sub-basin in the PEL. Indeed, a growing body of recent theoretical and modeling studies [10,24–27] also support the complexity and richness of the PEL in amorphous solids, by revealing that the bottoms of sub-basins are hierarchical and far from smooth. In particular, the "ripples" in the bottom of PEL discovered by Zella et al. [28] are found responsible to the NCL phenomenon. However, the origin of the "ripples" or other fine structures in the bottom of sub-basins remain elusive, which we seek to clarify in the present study.

Here, using atomistic simulation methods, we probe the smoothness of sub-basin bottoms in various 3D glass models by imposing small intra-cage cyclic mechanical perturbations and then measuring the net changes in atomic-level stress [29]. We find that in glassy systems with pairwise interaction (*e.g.* Lennard Jones-type models, modified Johnson model, *etc*) the changes in atomic-level stress exhibit sharp jumps only at critical strains when cage-breaking events occur, while under lower strains the stress changes remain negligible and invariant. This indicates a relatively smooth and featureless bottom in the sub-basins of PEL. However, in systems with many body-interaction (*e.g.* metallic glass model $Cu_{50}Zr_{50}$ using embedded-atom method, EAM [30]) the atomic-level stress changes are much larger and exhibit a continuous variation even before the first cage-breaking events, implying a qualitatively different and much more rugged intra-cage PEL. We discover that such a remarkable distinction is strongly correlated to the topology of individual atom's confinement zone, namely the spatial distribution features of its constraining force field under perturbation. Specifically, the pairwise interaction ensures a linear covariation between a perturbed individual atom's energy change and the system's global energy change, which leads to a smoothly varying and well-confined restoring force under perturbation. In stark contrast, many-body interaction would break such an energetic linear covariation and make the restoring force no longer confined for a significant portion (~30 %) of atoms in the system, leading to an inherently more rugged bottom in the PEL. These findings reveal a profound connection between a system's bonding nature and its underlying PEL, which sheds light on new ways to design and control amorphous materials.

2. Results

2.1. Intra-cage cyclic loading & net property changes

Fig. 1 delineates the protocol of our modeling analysis. Starting from a mechanically stable sub-basin state (achieved, for example, through energy minimization), we first apply an athermal affine loading of shear strain, denoted as γ, to the sample, followed by a relaxation treatment. Subsequently, an affine unloading and another relaxation are employed, driving the sample to its final state. We examine the changes in properties (denoted as δ) between this final state and the initial state as a function of the implemented initial shear strain, γ. The idea is that, if the bottom of the initial basin is smooth, then the loading/unloading operation should, in principle, be reversible, and the change of $\delta(\gamma)$ should be negligible, provided that γ is smaller than the sub-basin's width. To ensure our scope is restrained within the interior of the sub-basin – that is, before any cage-breaking events or β relaxations occur – we also monitor the topological changes in atoms' local packing environments. We do this by defining a step function $\Theta(\gamma)$, which examines the Voronoi indices [31] for those most displaced atoms (within the top 0.01 % window) after the loading/unloading operation. If any changes are detected, we consider a cage-breaking event to have occurred, setting $\Theta(\gamma)$ to 1. Otherwise, the sample is deemed to be well within the sub-basin, and $\Theta(\gamma)$ is set to be 0. Our analysis below on $\delta(\gamma)$ will hence be concentrated in the $\Theta(\gamma) = 0$ regime.

Fig. 2a below shows the typical results for a Kob-Andersen (K-A) glass model [32] consisting of 50,000 atoms, which is a very well-known pairwise interacting system. To concentrate on the mechanical properties, here $\delta(\gamma)$ is defined as follows. First, we calculate the root mean square (RMS), $RMS\left(\Delta\sigma^i[N]\right)$, of the individual atomic-level stress changes $\Delta\sigma^i \equiv \sigma^i_{fin} - \sigma^i_{ini}$. Note that here we only focus on the shear stress component along the loading direction. As seen in Fig. 2a, the occurrences of first cage-breaking events in different samples do not necessarily synchronize, due to the inherent randomness of atomic packing in glasses. That said, the variations of $\delta(\gamma)$ are qualitatively the same and exhibit strong correlation with $\Theta(\gamma)$. Notably, a significant jump of $\delta(\gamma)$ occurs precisely at the incipient cage-breaking strain, while at lower strain $\delta(\gamma)$ remains nearly flat. This jump is expected, as substantial atomic rearrangements take place during cage breaking, leading to

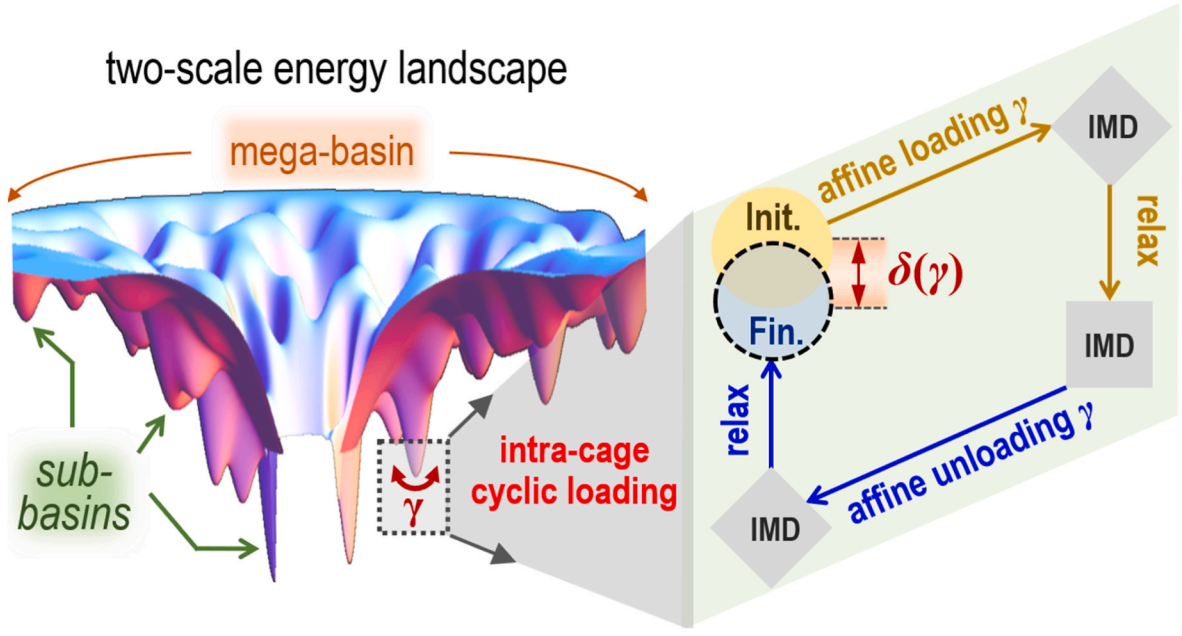

Fig. 1. Schematics of a two-scale energy landscape consisting of mega-basin and sub-basin. The present study focuses on the net changes in property under intra-cage cyclic loading to a sub-basin state.

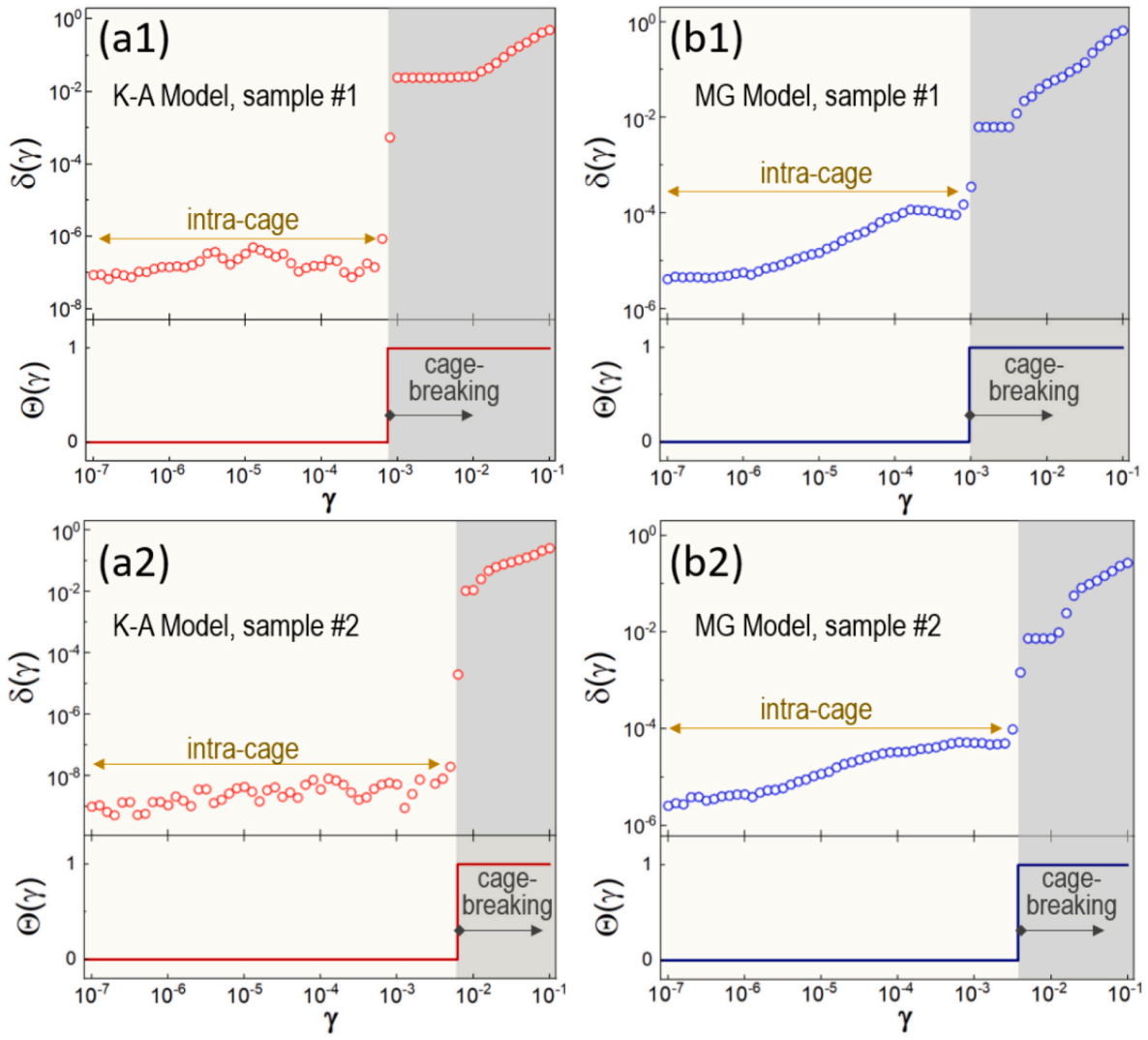

Fig. 2. The variations of $\delta(\gamma)$ in (a1-a2) two representative cases for the K-A model, and (b1-b2) two representative cases for the MG model, respectively.

considerable property changes. The nearly invariant behavior of $\delta(\gamma)$ in the intra-cage regime suggests a featureless bottom within the sub-basin.

For comparison, in Fig. 2c we present results from two typical metallic glass (MG) samples, which is a widely adopted many-body interacting system. Note that to facilitate the quantitative comparisons between various glass models, $RMS(\Delta\sigma^i[N])$ is further normalized to the RMS of the sample's own atomic-level stress at the initial state, defined as $\delta \equiv RMS(\Delta\sigma^i[N])/RMS(\sigma^i_{ini}\,[N])$. It can be seen that, although $\delta(\gamma)$ still exhibits an abrupt change at the cage-breaking strain, its intra-cage behavior differs significantly. Unlike the flat trend observed in the K-A model, $\delta(\gamma)$ in MG samples shows clear dependence on γ, indicating richer features at the sub-basin bottom.

2.2. Stark distinction between pairwise and many-body glasses

To gain a deeper perspective, in Fig. 3a we examine the histograms of individual atoms' stress changes in both the K-A and MG systems up to the cage-breaking points. Note that to make a meaningful comparison, the marked strains have been renormalized with respect to each sample's cage-breaking strain $\gamma_{c.b.}$, and to improve the statistical reliability each histogram represents the average results of 10 samples.

In the K-A model (Fig. 3 a1), the histograms are very narrowly distributed around zero and collapse with each other, until a sudden broadening of the distribution occurs at the cage-breaking strain. The inset plot tracks the variation of the full width at half maximum (FWHM) of the histograms, which shows an apparent step-like profile. In stark contrast, the MG model (Fig. 3 a2) exhibits distinct and continuously varying profiles even before cage breaking. As seen in the inset plot, the FWHM gradually broadens almost in a linear pattern in the log-log scale, indicating a scale-free power law between the intra-cage loading magnitude γ and the resultant property changes.

In addition to the K-A model, we have also examined other glasses with pairwise interaction, including a 50:50 LJ model with different parameters [33], as well as a modified Johnson model [34,35], which gives different asymmetry of the pair-interacting potential well from that of LJ type. To eliminate the potential size effect, here all the samples across different models have the same geometry and contain the same number of atoms (more details in **Sec. 4**). As depicted in Fig. 3b, although all the glass models exhibit quantitatively consistent behaviors beyond the cage-breaking strain, within the intra-cage regime, the results can be evidently divided into two distinct groups. Compared with the models with pairwise interaction where $\delta(\gamma)$ remains small and almost flat, in the MG model with many-body interaction the variations of $\delta(\gamma)$ are several orders of magnitude larger and, more importantly, dependent on the γ. This reflects a more complex sub-basin in MG that contains very fine structures/traps in the intra-cage PEL. And the origin of these subtle features naturally becomes a subsequent question to discuss below.

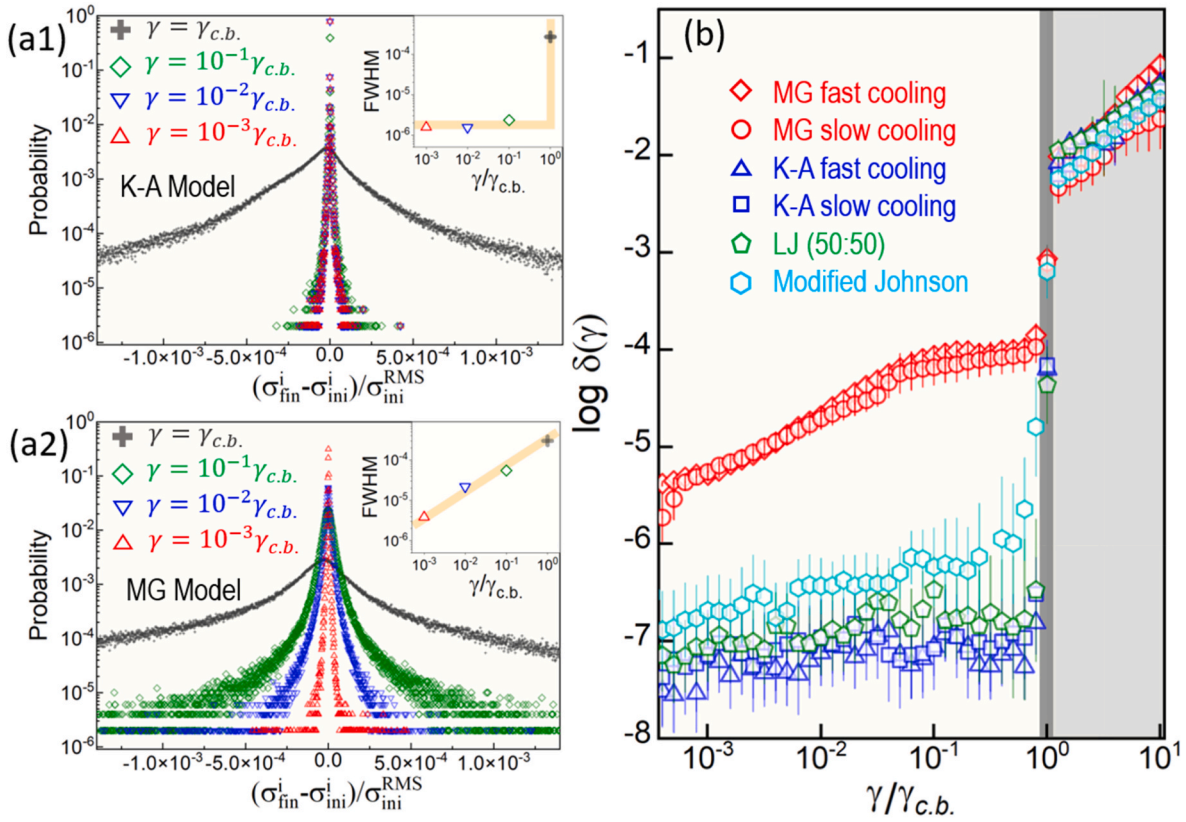

Fig. 3. Distributions of individual atomic-level stress changes $\Delta\sigma^i \equiv \sigma^i_{fin} - \sigma^i_{ini}$ after cyclic loadings at different levels of strain range relative to the cage-breaking strain $\gamma_{c.b.}$, for (a1) the K-A model, and (a2) the MG model. Inset plots represent the corresponding variations of FWHM of the histograms; (b) Quantitative comparisons on δ(γ) across various glass models. Each data point represents the average result of 10 independent samples, and vertical bars represent the standard errors based on the results of those 10 independent samples.

2.3. Topologies of constraining force-fields to individual atoms

A condensed matter system's behavior is ultimately comprised of the responses of individual atoms to external stimuli. Therefore, to tackle the problem, we first probe the topologies of the constraining force-field zones for individual atoms in various glass models (*i.e.* equivalently the local dynamical matrix). As illustrated in Fig. 4a, while fixing the spatial coordinates of all other atoms, we introduce small perturbations dr along various directions (θ, φ) to a selected atom and examine its resultant energy variation dE_{atom}. If the atom's energy increases (*i.e.* $dE_{atom} > 0$) it would mean a normal restoring force and thus an effective confinement; otherwise, the atom is not confined along the perturbing direction. And to focus on the intra-cage regime, the magnitude of $|dr|$ is set to be much smaller than the nearest neighbor distance (R_{NN}) of the sample. For the convenience of visualization, we employ the Mollweide projection [36] (see **Sec. 4** for details) to project the 3D information to a series of 2D maps at controlled $|dr|$ magnitudes. Fig. 4 b1-b2 shows the angular dependence of dE_{atom} for a typical selected atom in the K-A model and in the MG model, respectively. The most striking contrast is that, while in the K-A model dE_{atom} is positive-definite, in the MG model dE_{atom} can be negative along certain directions. Another noteworthy observation is that the fraction of the negative area does not shrink as $|dr|$ decreases, implying that the asymptotic behaviors of dE_{atom} upon vanishing perturbations are fundamentally different in the two models, and that in the MG model the confinement zones of individual atoms are inherently more complex and less bounded.

Such a distinction is also reflected in the profiles of cluster curves $dE_{atom}(dr)$ along different solid angles shown in Fig. 4 c1-c2. Clearly, in the K-A model all the curves are monotonically increasing, and the different ascending rates reflect the diverse confinement strengths along various directions that are expected in disordered solids. However, the MG model exhibits a qualitatively different behavior, as manifested by that a fraction of the curves turn negative first. It is worth emphasizing that, although the individual atom's energy variations dE_{atom} could be negative in MG model, the system's total energy variations dE_{sys} under the same perturbations are always positive-definite, as seen in the inset plots of Fig. 4c. On the one hand, such a positive definiteness of the total energy variation is entirely anticipated and required by physics, because as mentioned earlier all the samples are prepared via energy minimizations, meaning that they are initially located at mechanically stable states. On the other hand, the correlations between dE_{atom} and dE_{sys} are subjected to the detailed interatomic interactions. Specifically, consider a system that only comprises pairwise interactions:

$$E^i_{atom} = \frac{1}{2}\sum_{j\neq i}\phi_{\alpha\beta}(r_{ij}), E_{sys} = \sum_i E^i_{atom} = \sum_{i<j}\phi_{\alpha\beta}(r_{ij}) \quad (1)$$

Then, upon a small perturbation to atom i while keeping all other atoms fixed, there is a rigorous correlation of $dE_{sys} = 2dE^i_{atom}$ because each "bond" energy in the pairwise-interacting system is equally shared by two atoms. And this is the case seen in Fig. 4 c1. However, if many-body interactions are included in the system such as the EAM potential:

$$E^i_{atom} = \frac{1}{2}\sum_{j\neq i}\phi_{\alpha\beta}(r_{ij}) + F_\alpha\left(\sum_{j\neq i}\rho_\beta(r_{ij})\right), E_{sys} = \sum_i E^i_{atom} \quad (2)$$

Then the linear correlation between dE^i_{atom} and dE_{sys} no longer holds, because the embedded energy in the 2nd term attributed to atom i is not linearly shared with other atoms. In other words, due to this intrinsic many-body interaction, $F_\alpha\left(\sum_{j\neq i}\rho_\beta(r_{ij})\right)$, it becomes possible that $dE_{atom} < 0$ while $dE_{sys} > 0$. And such a breakdown of the simple linear

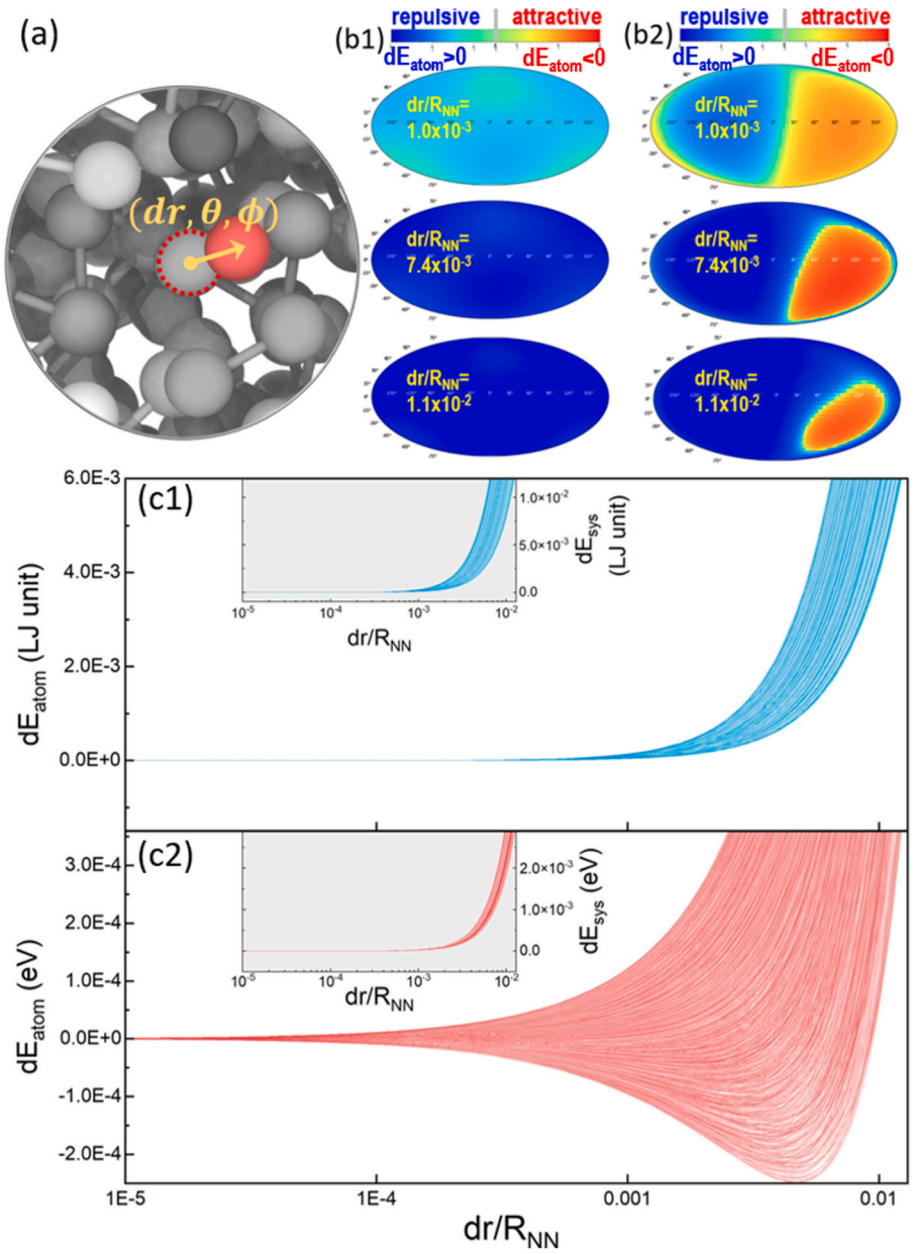

Fig. 4. (a) Probe of individual atom's constraining force field by introducing small perturbations in spherical coordinate while fixing all other atoms; Typical features of the probed force fields for (b1) the K-A model and (b2) the MG model, at the scaled distance of $dr/R_{NN} = 1.0*10^{-3}$, $7.4*10^{-3}$, and $1.1*10^{-2}$, respectively; The profiles of cluster curves of the perturbed atom's energy variations, $dE_{atom}(dr)$, along different solid angles for (c1) the K-A model and (c2) the MG model. Inset plots are the total energy variations of the whole system under the same perturbations, $dE_{sys}(dr)$.

coordination between dE_{atom} and dE_{sys} makes the constraining force fields of individual atoms fundamentally more complex in the MG model. In particular, the atoms become less confined and can in principle move even under vanishing perturbations. Notably, very recent in-situ coherent x-ray scattering by Maass's group [37] shows that MGs, while macroscopically stable, exhibit strong atomic-scale transport under essentially arbitrary low stress, corroborating our present results.

2.4. Statistics and spatial distributions of $\Omega(dE_{atom} < 0)$ zones in many-body glasses

In addition to probing the behaviors of a few representative atoms discussed above, we also conducted more statistical analysis. Specifically, Fig. 5a shows the histograms of the $dE_{atom} < 0$ occurrence probability – namely the corresponding solid angles to the negative energy variation zone $\Omega(dE_{atom}\langle 0 <)$ normalized by 4π – based on the scrutinization on the confinement zones of every individual atom in the MG model (see Sec.4 for details). The results exhibit broad distributions, and on average upon random perturbations to an individual atom there is about 30 % chance such an atom will lose the confinement and not return to its initial position. The broad distributions reflect that the spatial characteristics of constraining force fields to individual atoms in MGs are diverse, and a natural question to ask is whether or not there exists any correspondence between the individual atoms' local structures and those characteristics. With further data scrutinization (see Supplemental Materials), we discover that the atoms embedded in relatively high 5-fold-symmetry local environments may have lower abnormality of $\Omega(dE_{atom}\langle 0 <)$ compared with other atoms. However, the discovered dependence is rather weak and more like a propensity instead of a strong correlation. To extract more useful insights into the structure-property

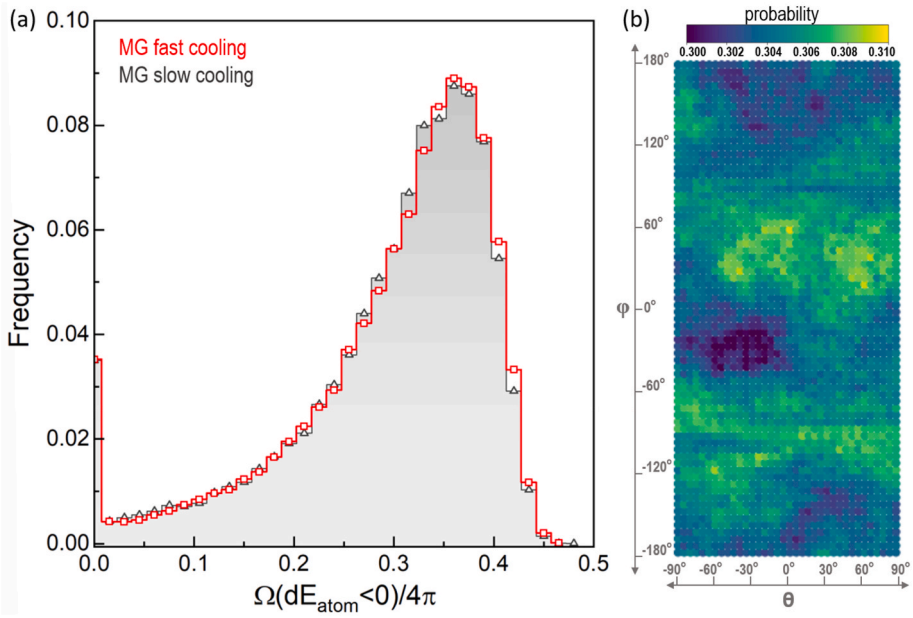

Fig. 5. (a) Histograms on the fractional occupancy of the corresponding solid angles with $dE_{atom} < 0$ features for perturbed atoms in the MG model; (b) Directional distributions of those $dE_{atom} < 0$ areas in the (θ, φ) space for all atoms.

relationship near the bottom of the energy landscape, some data-driven techniques such as interpretable machine learning algorithm [38] may be warranted.

The effect of sample's processing history is also probed. We discover that, compared with a fast quenched sample, a relatively slowly cooled sample presents a histogram that is slightly shifted toward the left, indicating an enhanced level of confinement. However, such a shift is rather weak, implying that the widely populated $dE_{atom} < 0$ spots and the lack of confinement to perturbed atoms are intrinsic features in the many-body MG model. Notably, such a weak cooling rate dependence inside a sub-basin is in stark contrast to the known strong effect of cooling rate on the entire energy landscape, such as the density and distribution of sub-basins [13,39], as well as the aging/rejuvenation behaviors [20,40]. Therefore, the present results indicate a new governing physics in the intra-cage regime.

In Fig. 5b we also examine the directional distributions of those $dE_{atom} < 0$ areas in the (θ, φ) space for all atoms. A relatively uniform distribution is observed, and along each specified direction there are on average 30 % atoms exhibiting the $dE_{atom} < 0$ behavior upon perturbation. This is not surprising, because the samples considered in the present work are thermally prepared (and then minimized), and hence a statistical isotropy should be expected. It would be of interest to probe how external (deviatoric) loadings would impact such an isotropy, although it is beyond the scope of the present work and will be discussed in a future study.

3. Discussions and conclusion

To summarize, by examining the behaviors of various energy-minimized glassy samples under small intra-cage cyclic loadings we discover that the MG model exhibits a fundamentally distinct performance from that in the glass models with pairwise interaction (*e.g.* Fig. 3b). In particular, the bottoms of sub-basins in the PEL of MG model are inherently non-smooth. We further demonstrate that the smoothness of sub-basin bottoms is closely related to the nature of the interatomic potential. Specifically, upon single-atom perturbations, for pairwise interatomic potentials both the perturbed atom's energy variation and the overall sample' energy variation are positive-definite, and there exists a rigorous linear coordination as $dE_{sys} = 2dE_{atom}$. This means that under infinitesimal stimuli each individual atom is well-confined and intended to return to its original position. In other words, the very bottom of PEL is smooth. However, in the presence of embedded many-body interactions, the linear synchrony between dE_{atom} and dE_{sys} is not longer guaranteed. And there is intrinsically ~30 % chance, at least for the EAM-typed interaction we consider here in the present study, that the perturbed atom is no longer confined (*i.e.* $dE_{atom} < 0$) while the overall sample's energy variation is still positive-definite (*i.e.* $dE_{sys} > 0$). In other words, the sub-basins bottoms are no longer smooth, and some very fine structures, *i.e.* the "ripples" [28], would emerge. This explains why the MG model does not return to the initial state as other pairwise models do after small intra-cage cyclic loading. It is worth clarifying that both MG model [39] and models with pairwise-interaction [41,42] are known to have globally rugged PEL that consists of countless sub-basins (*i.e.* inherent structures) with the barrier heights distributed down to nearly zero, and the distinction of PEL smoothness discussed here in the present study lies only within the interior of a sub-basin.

Interestingly, recent studies on the jamming transition in glassy materials also show that existence of marginal phase is not guaranteed but sensitively dependent on the bonding nature of the constituent particles. In particular, the Gardner transition discovered in the hard-sphere glass model, as well as its associated marginal stability and fractal energy landscape [24], may disappear under continuous pairwise interactions [43,44]. These studies are in line with the findings in our present work. Such an agreement is encouraging because it not only reveals the profound roles of atomic interactions in dictating the physical behaviors of glassy systems, but also stimulate new experiments to control the properties of amorphous materials. For example, the many-body interaction in MGs stems from itinerant electrons [45,46]. Local electronic orbitals are strongly affected by the neighbors through orbital hybridization (ligand-field effects), and small changes in local structure can have significant effects on the local electronic states. Such local interactions are many-body in nature, and provide added degrees of freedom, not represented by pairwise interactions. It is possible that such additional degrees of freedom contribute to the increased complexity at the bottom of the PEL basins. Therefore, by exploiting various chemical elements to tune such local electronic states – *e.g.* covalent vs. metallic – one may modulate the density and magnitude of the "ripples", and, subsequently, the dissipations via the NCL phenomenon. In addition to MGs, there also exist many other amorphous systems

where many-body interaction could play an indispensable role, such as the interaction between charged colloids with long screening lengths [47,48], colloid-polymer mixture with depletion effect [49], space-tiling cells from foam and tissues [50], highly deformable particles [51], as well as granular particles mediated with an interstitial fluid [52]. Hence, the insights obtained from the present study may also be broadly applicable to a range of important materials and problems. We would like to mark that here we mainly considered the effects of bonding natures but did not examine the thermal effect. At finite temperature, the non-vibrational entropy could impose another layer of complexity to the fine structures near the bottom of energy landscape [53]. And the compounding effect of many-body interaction and entropy term would warrant future investigation.

As a final remark, it is worth noting that the basic functions in the EAM potential used here for the MG model [30] – namely $\phi_{\alpha\beta}$, ρ_β, and F_α in Eq. (2) – are actually all smooth and differentiable. Therefore, a natural question arises is that how come these smooth bases could build up an inherently non-smooth and infinitely rugged energy landscape. We would like to remark that such a scenario, although not immediately intuitive, is indeed possible. For example, consider a well-known Weierstrass function $W(x) = \sum_{n=0}^{\infty} a^n \cos(b^n \pi x)$, $0 < a < 1$, which is bounded and consists of only simple and smooth $\cos(x)$ function series. It is known that [54,55] the smoothness of such Weierstrass function is not guaranteed and depends on the coefficients a and b: under the circumstance of $ab<1$, $W(x)$ is a regular curve with continuous derivative; while in case of $ab>1$, the function becomes fractal, namely continuous everywhere but differentiable nowhere. In a physical system, the restoring force is essentially the derivative of the underlying PEL. Therefore, once the PEL becomes fractal the restoring force can no longer be well defined, and, subsequently, arbitrary small perturbations would drive the system leaving its initial state. In other words, even though the elemental functions $\phi_{\alpha\beta}$, ρ_β, and F_α are all smooth, there is reason to speculate that the system's structural order or disorder could modulate the coefficients in front of those elements and lead to different natures of the global PEL. To validate this idea, we examine a B2 crystalline structure of the Cu-Zr alloy using the exact same EAM potential. As seen in Fig. 6, both dE_{atom} and dE_{sys} are clearly positive definite, indicating effective confinements to individual atoms under infinitesimal perturbations and hence a smooth bottom of the PEL. In a nutshell, the non-smoothness of the sub-basins in MGs is an outcome due to the mutual impacts of structural disorder and many-body interaction. Admittedly, this further raises a new intriguing question, that is, what is the critical level of structural disorder that the PEL switches from smooth to fractal? It is beyond the scope of the present work and warrants future investigations.

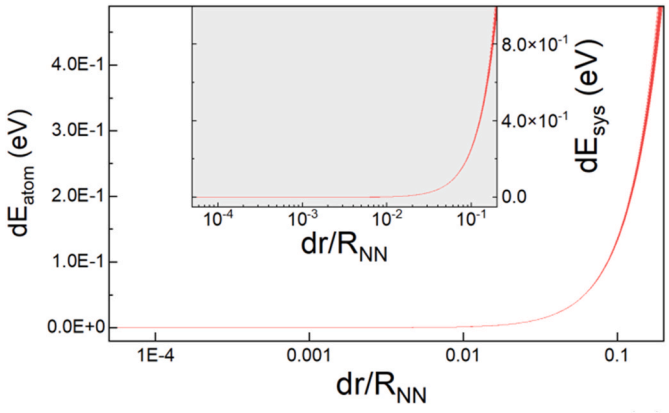

Fig. 6. The profiles of cluster curves of the perturbed atom's energy variations, $dE_{atom}(dr)$, along different solid angles for the B2 CuZr model. Inset plots are the total energy variations of the whole system under the same perturbations, $dE_{sys}(dr)$.

4. Methods and materials

4.1. Model set up

Four different glass models with various types of interatomic potentials are set up and investigated using the Large-scale Atomic/Molecular Massively Parallel Simulator (LAMMPS) software [56,57]. To eliminate the potential size effect and ensure a meaningful comparative study, all the simulation samples across various models are set to contain the same number of atoms (*i.e.* 50,000 in the present study) and have the same geometry of simulation box (*i.e.* the x:y:z ratio). In particular, (i) for the many-body MG model, we adopt the EAM-type potential [30] at the composition of $Cu_{50}Zr_{50}$ with the simulation box size of 163.4 × 32.68 × 163.4 Å^3. We generate two sets of samples at different cooling rates of 10^{13} K/s and 10^{11} K/s, respectively. Each set includes 10 independent samples that are first equilibrated at 2000 K for 10 ns and then quenched to 0 K; (ii) for the K-A model [32], we adopt a classical 80:20 partition of particles with the simulation box size of 52.15 × 10.43 × 52.15 (LJ unit). We also consider two different cooling rates at 10^{-3} and 10^{-5} (LJ unit), and similarly as in MG model, 10 independent samples are prepared at each cooling rate by quenching a high-temperature (T = 5.0, LJ unit) equilibrated liquid; (iii) another LJ-type glass model with 50:50 composition [33] is set up with the size of 52.15 × 10.43 × 52.15 (LJ unit), and 10 independent samples are prepared with the cooling rate of 2 × 10^{-2} (LJ unit); and, (iv) a modified Johnson pairwise glass model [34,35] is also set up with the size of 143 × 28.6 × 143 Å^3, and 10 independent samples are prepared via fast quenching at 10^{14} K/s. Periodical boundary conditions (PBC) are applied to all the above-mentioned samples. The atomic-level stress tensor used in Figs. 2 and 3 above is calculated by $\sigma_i^{ab} = -\frac{1}{2\Omega_i}\sum_{j\neq i} f_{ij}\frac{r_{ij}^a r_{ij}^b}{r_{ij}}$ [58].

It is worth noting that, the four different models considered here are quite generic, and they have been widely employed to represent a diverse array of glassy materials. In this sense, we therefore believe that the key findings in our present study are broadly applicable. That said, in the future it is still beneficial to conduct a full-scope and more comprehensive study, by including other types of glassy models. For example, in addition to the isotropic bonding considered here, one might also want to probe some other special forms of atomic interactions, such as the Stillinger-Weber type [59] anisotropic three-body bonding model, *etc*.

4.2. Mollweide projection

In the measurement of energy variations under single-atom perturbations, the small displacement given to the selected atom is controlled in spherical coordinate notation $\boldsymbol{dr}(dr,\theta,\phi)$, as illustrated in Fig. 7a. With a fixed dr, the sampling points are uniformly distributed in the (θ,ϕ) space, as seen in Fig. 7b. Finally, a mapping to Fig. 7c, namely $(\theta,\phi)\rightarrow(x, y)$, is conducted via the Mollweide projection algorithm:

$$x = \frac{2\sqrt{2}}{\pi}\theta\cos\alpha$$

$$y = \sqrt{2}\sin\alpha$$

where α is auxiliary angle defined by

$$2\alpha + \sin 2\alpha = \pi\sin\phi$$

This is how Fig. 4b was constructed in **Sec. 2** above.

4.3. Distributions of the $dE_{atom}^i < 0$ occurrence probability

As illustrated above in **Sec. 4.2**, for each individual atom, at a given selection of dr (to be discussed below), we examine such perturbed atom's energy variations dE_{atom}^i along various directions in the (θ,φ)

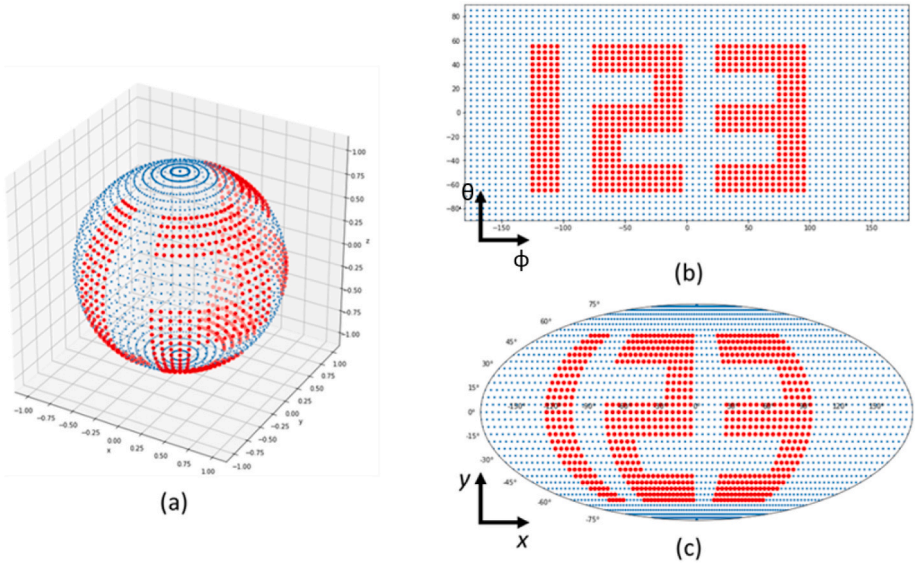

Fig. 7. Converting data on a spherical shell to Mollweide projection. (a) Data point positions in 3D space; (b) 2D plot with respect to angular data (θ, ϕ) (c) 2D plot with Mollweide projection. Pattern with the shape of digits is used only for demonstration.

space. In particular, we measure the corresponding solid angles to the negative energy variation $dE^i_{atom} < 0$, defined as:

$$\Omega^i\left(dr, dE^i_{atom} < 0\right) = \sum_{\phi}\sum_{\theta} H\left(-dE^i_{atom}(dr, \theta, \phi)\right) \int_{\phi-\delta\phi/2}^{\phi+\delta\phi/2} \int_{\theta-\delta\theta/2}^{\theta+\delta\theta/2} \sin\theta d\theta d\phi$$

where $H(\cdot)$ is the Heaviside function determining whether the energy change is smaller than 0, and the integral part calculate the solid angle occupied by the specific direction with $\delta\theta, \delta\phi$ represent the sampling distance of θ and ϕ.

The so-obtained Ω^i, further scaled by the total solid angle of 4π, thus represents the occurrence probability of atom i losing confinement under perturbations. For each individual atom, there is such an associated probability, and Fig. 5a in **Sec. 2** above represents the histogram of such probability distributions by scrutinizing all the atoms in the sample. To conduct the above-mentioned measurements, one has to first select a value of perturbed distance dr for the analysis. It is worth emphasizing that, different selection of dr would only cause slight quantitative changes of the results but will not affect the main conclusion of the present study, namely the nature of infinitely rugged intra-cage PEL in MG model.

More specifically in our analysis, the selection of dr was determined the following way: as seen in Fig. 4 c2 in **Sec. 2**, for each perturbed atom, its energy variation δE_{atom} exhibits a minimum at certain displacement of dr. One could then use the statistical nature of such $dr\left(\delta E^{min}_{atom}\right)$ to guide the selection of a characteristic dr. Fig. 8 below shows the histogram of the $dr\left(\delta E^{min}_{atom}\right)$ for the MG model concerned in the present study, where a peak near 0.01 *Å* occurs. And the results in Fig. 5 in the main text were hence obtained based on such a selection of dr.

Fig. 8 essentially reflects that the constraining force fields to individual atoms in MGs are not identical and exhibit a broad distribution. There is reason to speculate such a constraining force fields heterogeneity must be originated from some sort of "structural inhomogeneity" at atomic level. As mentioned above in **Sec. 2.4**, with further data scrutinization (see Supplemental Materials), we discover a weak propensity between the local 5-fold-symmetry and the abnormality of $\Omega(\mathrm{dE_{atom}}\langle 0 <)$. However, a strong structure-property relationship is yet to be built. It is also worth clarifying that, the structural heterogeneity mentioned above is within the intra-cage regime, which is different from the cage-breaking events-associated structural heterogeneity and the so-caused deformation and relaxation behaviors [60,61].

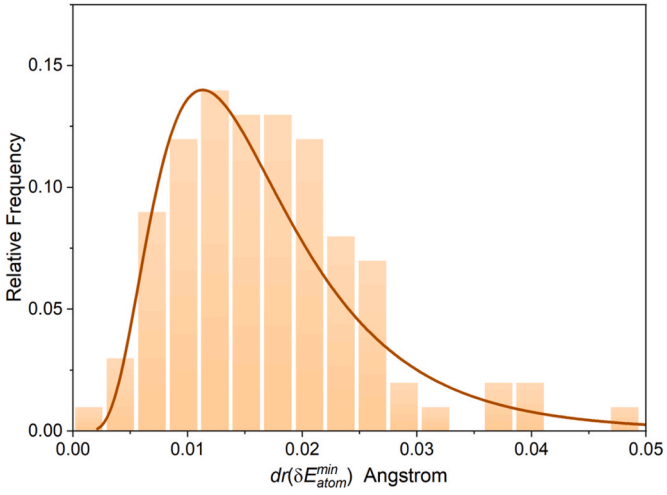

Fig. 8. The histogram of dr distribution where $\min\{\delta E_{atom}\}$ occurs.

4.4. *Effects of bonding nature on the correlations between* $\mathbf{dE}_{atom}$ *and* $\mathbf{dE}_{sys}$

(a) For pairwise-interacting system: The individual atom's energy and the whole system's energy can be expressed as:

$$E^i_{atom}(r_{ij}) = \frac{1}{2}\sum_{j\neq i}\phi_{\alpha\beta}(r_{ij}),$$

$$E_{sys}(\boldsymbol{r}^{3N}) = \sum_i E^i_{atom} = \frac{1}{2}\sum_i\sum_{j\neq i}\phi_{\alpha\beta}(r_{ij}) = \sum_{i,j\ (i<j)}\phi_{\alpha\beta}(r_{ij})$$

where $\phi_{\alpha\beta}(r_{ij})$ represents the bonding energy between i-j pair and could in principle adopt any formulism. Now consider a small perturbation to atom i while keeping all other atoms fixed, which causes a pair distance update $r_{ij} \rightarrow r^0_{ij} + \delta r_{ij}$ for all bonds connected to atom i, then the atom i's energy change can be written as:

$$\delta E^i_{atom} = \frac{1}{2}\sum_{j\neq i}\left[\left.\frac{\partial \phi_{\alpha\beta}(r_{ij})}{\partial \boldsymbol{r_{ij}}}\right|_{r^0_{ij}} \delta \boldsymbol{r}_{ij} + \frac{1}{2}\left.\frac{\partial^2 \phi_{\alpha\beta}(r_{ij})}{\partial \boldsymbol{r_{ij}}^2}\right|_{r^0_{ij}} (\delta \boldsymbol{r}_{ij})^2 + \ldots\right]$$

As for the energy change of the whole system, among the total of $N(N-1)/2$ bonds, only those directly connected to atom i would undergo an energy variation under such a perturbation. And there is:

$$\delta E_{sys} = \sum_{j\neq i}\left[\left.\frac{\partial \phi_{\alpha\beta}(r_{ij})}{\partial \boldsymbol{r_{ij}}}\right|_{r^0_{ij}} \delta \boldsymbol{r}_{ij} + \frac{1}{2}\left.\frac{\partial^2 \phi_{\alpha\beta}(r_{ij})}{\partial \boldsymbol{r_{ij}}^2}\right|_{r^0_{ij}} (\delta \boldsymbol{r}_{ij})^2 + \ldots\right] = 2\delta E^i_{atom}$$

In other words, there is a rigorous linear covariation between the two variables as $\delta E_{sys} = 2\delta E^i_{atom}$. Since the glass samples are prepared via energy minimizations, the total energy change of the whole system under arbitrary perturbation would have to be positive definite (*i.e.* $dE_{sys} > 0$). And consequently, due to the above-derived rigorous linear covariation, the perturbed atom's energy change would also have to be always positive definite (*i.e.* $\delta E^i_{atom} > 0$). In other words, under vanishing perturbations, the perturbed atom always undergoes well-defined constraining force field and intends to move back to the original position.

(b) For many-body interacting system: Consider an embedded-atom method (EAM) potential, which has been widely used to describe the many-body interacting metallic glasses, the individual atom's energy and the whole system's energy are written as:

$$E^i_{atom} = \frac{1}{2}\sum_{j\neq i}\phi_{\alpha\beta}(r_{ij}) + F_\alpha\left(\sum_{j\neq i}\rho_\beta(r_{ij})\right), E_{sys} = \sum_i E^i_{atom}$$

Similarly as above, under a perturbation to atom i, its energy change would be:

$$\delta E^i_{atom} = \frac{1}{2}\sum_{j\neq i}\left[\left.\frac{\partial \phi_{\alpha\beta}(r_{ij})}{\partial \boldsymbol{r_{ij}}}\right|_{r^0_{ij}} \delta \boldsymbol{r}_{ij} + \frac{1}{2}\left.\frac{\partial^2 \phi_{\alpha\beta}(r_{ij})}{\partial \boldsymbol{r_{ij}}^2}\right|_{r^0_{ij}} (\delta \boldsymbol{r}_{ij})^2 + \ldots\right]$$

$$+F'_\alpha\big|_{r^0_{ij}} \cdot \sum_{j\neq i}\left.\frac{\partial \rho_\beta(r_{ij})}{\partial r_{ij}}\right|_{r^0_{ij}} \delta \boldsymbol{r}_{ij} + \ldots$$

And for the energy change of the whole system there is:

$$\delta E_{sys} = \sum_{j\neq i}\left[\left.\frac{\partial \phi_{\alpha\beta}(r_{ij})}{\partial \boldsymbol{r_{ij}}}\right|_{r^0_{ij}} \delta \boldsymbol{r}_{ij} + \frac{1}{2}\left.\frac{\partial^2 \phi_{\alpha\beta}(r_{ij})}{\partial \boldsymbol{r_{ij}}^2}\right|_{r^0_{ij}} (\delta \boldsymbol{r}_{ij})^2 + \ldots\right]$$
$$+\sum_i F'_\alpha\big|_{r^0_{ij}} \cdot \sum_{j\neq i}\left.\frac{\partial \rho_\beta(r_{ij})}{\partial r_{ij}}\right|_{r^0_{ij}} \delta \boldsymbol{r}_{ij} + \ldots$$

Due to the intrinsic many-body interaction, $F_\alpha\left(\sum_{j\neq i}\rho_\beta(r_{ij})\right)$, there is no guaranteed simple covariation between the term $F'_\alpha\big|_{r^0_{ij}} \cdot \sum_{j\neq i}\left.\frac{\partial \rho_\beta(r_{ij})}{\partial r_{ij}}\right|_{r^0_{ij}} \delta \boldsymbol{r}_{ij}$ and the term $\sum_i F'_\alpha\big|_{r^0_{ij}} \cdot \sum_{j\neq i}\left.\frac{\partial \rho_\beta(r_{ij})}{\partial r_{ij}}\right|_{r^0_{ij}} \delta \boldsymbol{r}_{ij}$. In other words, it becomes possible that $dE_{atom} < 0$ while $dE_{sys} > 0$. And such a breakdown of the simple linear coordination between dE_{atom} and dE_{sys} makes the constraining force fields of individual atoms fundamentally more complex in the MG model. In particular, the atoms become less confined and can in principle move even under vanishing perturbations.

CRediT authorship contribution statement

Haoyu Li: Writing – original draft, Visualization, Methodology, Investigation, Formal analysis, Data curation. **Hongyi Xiao:** Writing – review & editing, Writing – original draft, Resources, Conceptualization. **Takeshi Egami:** Writing – review & editing, Writing – original draft, Validation. **Yue Fan:** Writing – review & editing, Writing – original draft, Supervision, Resources, Investigation, Funding acquisition, Formal analysis, Conceptualization.

Declaration of competing interest

The authors declare that they have no known competing financial interests or personal relationships that could have appeared to influence the work reported in this paper.

Acknowledgements

HX and YF thank the support of START grant project by University of Michigan. The work by TE was supported by the US Department of Energy, Office of Science, Basic Energy Sciences, Materials Science and Engineering Division. YF also acknowledges the support by NSF under Grant No. DMR-1944879.

Appendix A. Supplementary data

Supplementary data to this article can be found online at https://doi.org/10.1016/j.mtphys.2024.101582.

Data availability

Data will be made available on request.

References

[1] D.C. Hofmann, et al., Designing metallic glass matrix composites with high toughness and tensile ductility, Nature 451 (7182) (2008) 1085–1089.
[2] J.-O. Krisponeit, et al., Crossover from random three-dimensional avalanches to correlated nano shear bands in metallic glasses, Nat. Commun. 5 (2014).
[3] D. Rodney, C. Schuh, Distribution of thermally activated plastic events in a flowing glass, Phys. Rev. Lett. 102 (23) (2009): 235503.
[4] Y. Fan, T. Iwashita, T. Egami, Crossover from localized to cascade relaxations in metallic glasses, Phys. Rev. Lett. 115 (4) (2015): 045501.
[5] H.-N. Lee, K. Paeng, S.F. Swallen, M.D. Ediger, Direct measurement of molecular mobility in actively deformed polymer glasses, Science 323 (5911) (2009) 231–234.
[6] A.N. Raegen, J. Yin, Q. Zhou, J.A. Forrest, Ultrastable monodisperse polymer glass formed by physical vapour deposition, Nat. Mater. 19 (10) (2020) 1110–1113.
[7] R.A. Riggleman, H.-N. Lee, M.D. Ediger, J.J. de Pablo, Free volume and finite-size effects in a polymer glass under stress, Phys. Rev. Lett. 99 (21) (2007): 215501.
[8] P. Schall, D.A. Weitz, F. Spaepen, Structural rearrangements that govern flow in colloidal glasses, Science 318 (5858) (2007) 1895–1899.
[9] V. Chikkadi, G. Wegdam, D. Bonn, B. Nienhuis, P. Schall, Long-range strain correlations in sheared colloidal glasses, Phys. Rev. Lett. 107 (19) (2011): 198303.
[10] H.J. Hwang, R.A. Riggleman, J.C. Crocker, Understanding soft glassy materials using an energy landscape approach, Nat. Mater. 15 (9) (2016) 1031–1036.
[11] D.V. Denisov, K.A. Lörincz, J.T. Uhl, K.A. Dahmen, P. Schall, Universality of slip avalanches in flowing granular matter, Nat. Commun. 7 (1) (2016): 10641.
[12] P.G. Debenedetti, F.H. Stillinger, Supercooled liquids and the glass transition, Nature 410 (6825) (2001) 259–267.
[13] Y. Fan, T. Iwashita, T. Egami, How thermally activated deformation starts in metallic glass, Nat. Commun. 5 (2014) 5083.
[14] Y.Q. Cheng, E. Ma, Configurational dependence of elastic modulus of metallic glass, Phys. Rev. B 80 (6) (2009): 064104.
[15] Z. Wang, K.L. Ngai, W.H. Wang, S. Capaccioli, Coupling of caged molecule dynamics to Johari-Goldstein β-relaxation in metallic glasses, J. Appl. Phys. 119 (2) (2016): 024902.
[16] H.-B. Yu, et al., Fundamental link between β relaxation, excess wings, and cage-breaking in metallic glasses, J. Phys. Chem. Lett. 9 (19) (2018) 5877–5883.
[17] Q. Wang, et al., Unusual fast secondary relaxation in metallic glass, Nat. Commun. 6 (2015) 7876.
[18] D.P. Wang, J.C. Qiao, C.T. Liu, Relating structural heterogeneity to β relaxation processes in metallic glasses, Materials Research Letters 7 (8) (2019) 305–311.
[19] J.C. Ye, J. Lu, C.T. Liu, Q. Wang, Y. Yang, Atomistic free-volume zones and inelastic deformation of metallic glasses, Nat. Mater. 9 (8) (2010) 619–623.
[20] Y. Fan, T. Iwashita, T. Egami, Energy landscape-driven non-equilibrium evolution of inherent structure in disordered material, Nat. Commun. 8 (2017): 15417.
[21] K. Geirhos, P. Lunkenheimer, A. Loidl, Johari-goldstein relaxation far below ${T}_{g}$: experimental evidence for the gardner transition in structural glasses? Phys. Rev. Lett. 120 (8) (2018): 085705.
[22] L. Zella, J. Moon, D. Keffer, T. Egami, Transient nature of fast relaxation in metallic glass, Acta Mater. 239 (2022): 118254.

[23] T. Egami, T. Iwashita, W. Dmowski, Mechanical properties of metallic glasses, Metals 3 (1) (2013).
[24] P. Charbonneau, J. Kurchan, G. Parisi, P. Urbani, F. Zamponi, Fractal free energy landscapes in structural glasses, Nat. Commun. 5 (2014) 3725.
[25] P. Cao, M.P. Short, S. Yip, Potential energy landscape activations governing plastic flows in glass rheology, Proc. Natl. Acad. Sci. USA 116 (38) (2019): 18790.
[26] C. Liu, Y. Fan, Emergent fractal energy landscape as the origin of stress-accelerated dynamics in amorphous solids, Phys. Rev. Lett. 127 (21) (2021): 215502.
[27] L. Berthier, et al., Gardner physics in amorphous solids and beyond, J. Chem. Phys. 151 (1) (2019).
[28] L. Zella, J. Moon, T. Egami, Ripples in the bottom of the potential energy landscape of metallic glass, Nat. Commun. 15 (1) (2024) 1358.
[29] T. Egami, Atomic level stresses, Prog. Mater. Sci. 56 (6) (2011) 637–653.
[30] Y.Q. Cheng, E. Ma, H.W. Sheng, Atomic level structure in multicomponent bulk metallic glass, Phys. Rev. Lett. 102 (24) (2009): 245501.
[31] C.H. Rycroft, VORO++: a three-dimensional Voronoi cell library in C++, Chaos: An Interdisciplinary Journal of Nonlinear Science 19 (4) (2009): 041111.
[32] W. Kob, H.C. Andersen, Scaling behavior in the \ensuremath{\beta}$-Relaxation regime of a supercooled Lennard-Jones mixture, Phys. Rev. Lett. 73 (10) (1994) 1376–1379.
[33] U.R. Pedersen, T.B. Schrøder, J.C. Dyre, Phase diagram of kob-andersen-type binary Lennard-Jones mixtures, Phys. Rev. Lett. 120 (16) (2018): 165501.
[34] D. Srolovitz, K. Maeda, V. Vitek, T. Egami, Structural defects in amorphous solids Statistical analysis of a computer model, Philos. Mag. A 44 (4) (1981) 847–866.
[35] T. Iwashita, T. Egami, Atomic mechanism of flow in simple liquids under shear, Phys. Rev. Lett. 108 (19) (2012): 196001.
[36] J.P. Snyder, Flattening the Earth : Two Thousand Years of Map Projections, ed Ed, University of Chicago Press, Chicago, 1998. English) Paperback.
[37] R. Maaß, Communication at 2024 TMS Conference (2024).
[38] C. Liu, et al., Concurrent prediction of metallic glasses' global energy and internal structural heterogeneity by interpretable machine learning, Acta Mater. 259 (2023): 119281.
[39] C. Liu, P. Guan, Y. Fan, Correlating defects density in metallic glasses with the distribution of inherent structures in potential energy landscape, Acta Mater. 161 (2018) 295–301.
[40] C. Liu, X. Yan, P. Sharma, Y. Fan, Unraveling the non-monotonic ageing of metallic glasses in the metastability-temperature space, Comput. Mater. Sci. 172 (2020): 109347.
[41] S. Sastry, P.G. Debenedetti, F.H. Stillinger, Signatures of distinct dynamical regimes in the energy landscape of a glass-forming liquid. (Translated from English), Nature 393 (6685) (1998) 554–557 (in English).
[42] A. Kushima, et al., Computing the viscosity of supercooled liquids, J. Chem. Phys. 130 (22) (2009): 224504.
[43] C. Scalliet, L. Berthier, F. Zamponi, Absence of marginal stability in a structural glass, Phys. Rev. Lett. 119 (20) (2017): 205501.
[44] C.L. Hicks, M.J. Wheatley, M.J. Godfrey, M.A. Moore, Gardner transition in physical dimensions, Phys. Rev. Lett. 120 (22) (2018): 225501.
[45] S.M. Foiles, M.I. Baskes, M.S. Daw, Embedded-atom-method functions for the fcc metals Cu, Ag, Au, Ni, Pd, Pt, and their alloys, Phys. Rev. B 33 (12) (1986) 7983–7991.
[46] M.W. Finnis, J.E. Sinclair, A simple empirical N-body potential for transition metals, Philos. Mag. A 50 (1) (1984) 45–55.
[47] J.W. Merrill, S.K. Sainis, E.R. Dufresne, Many-body electrostatic forces between colloidal particles at vanishing ionic strength, Phys. Rev. Lett. 103 (13) (2009): 138301.
[48] J. Dobnikar, Y. Chen, R. Rzehak, Grünberg Hhv, Many-body interactions in colloidal suspensions, J. Phys. Condens. Matter 15 (1) (2003): S263.
[49] A.I. Chervanyov, G. Heinrich, Potential theory of the depletion interaction in the colloid-polymer mixtures, J. Chem. Phys. 131 (23) (2009).
[50] D.M. Sussman, M. Paoluzzi, Marchetti M. Cristina, M. Lisa Manning, Anomalous glassy dynamics in simple models of dense biological tissue, Europhys. Lett. 121 (3) (2018): 36001.
[51] J.A. Dijksman, T. Mullin, Creep control in soft particle packings, Phys. Rev. Lett. 128 (23) (2022): 238002.
[52] H. Xiao, A.J. Liu, D.J. Durian, Probing gardner physics in an active quasithermal pressure-controlled granular system of noncircular particles, Phys. Rev. Lett. 128 (24) (2022): 248001.
[53] M. Ozawa, A. Ikeda, K. Miyazaki, W. Kob, Ideal glass states are not purely vibrational: insight from randomly pinned glasses, Phys. Rev. Lett. 121 (20) (2018): 205501.
[54] B.R. Hunt, The Hausdorff Dimension of Graphs of Weierstrass Functions, Proceedings of the American Mathematical Society 126 (1998) 791–800.
[55] C. Gao, H. Zhai, Z.-Y. Shi, Dynamical fractal in quantum gases with discrete scaling symmetry, Phys. Rev. Lett. 122 (23) (2019): 230402.
[56] S. Plimpton, Fast Parallel algorithms for short-range molecular dynamics, J. Comput. Phys. 117 (1) (1995) 1–19.
[57] A.P. Thompson, et al., Lammps - a flexible simulation tool for particle-based materials modeling at the atomic, meso, and continuum scales, Comput. Phys. Commun. 271 (2022): 108171.
[58] Y. Fan, T. Iwashita, T. Egami, Evolution of elastic heterogeneity during aging in metallic glasses, Phys. Rev. 89 (6) (2014): 062313.
[59] F.H. Stillinger, T.A. Weber, Computer simulation of local order in condensed phases of silicon, Phys. Rev. B 31 (8) (1985) 5262–5271.
[60] L.T. Zhang, et al., Creep deformation in metallic glasses: a global approach with strain as an indicator within transition state theory, Int. J. Plast. 174 (2024): 103923.
[61] M. Popović, T.W.J. de Geus, W. Ji, A. Rosso, M. Wyart, Scaling description of creep flow in amorphous solids, Phys. Rev. Lett. 129 (20) (2022): 208001.